Astrophysics and Space Science (2007) **308**: 353–361 / **Corrected electronic version: September 4, 2007**

Alexander Y. Potekhin · Gilles Chabrier · Dmitry G. Yakovlev

Heat Blanketing Envelopes and Thermal Radiation of Strongly Magnetized Neutron Stars

arXiv:astro-ph/0611014v3 4 Sep 2007

Received: July 5, 2006 / Accepted: October 31, 2006

Abstract Strong ($B \gg 10^9$ G) and superstrong ($B \gtrsim 10^{14}$ G) magnetic fields profoundly affect many thermodynamic and kinetic characteristics of dense plasmas in neutron star envelopes. In particular, they produce strongly anisotropic thermal conductivity in the neutron star crust and modify the equation of state and radiative opacities in the atmosphere, which are major ingredients of the cooling theory and spectral atmosphere models. As a result, both the radiation spectrum and the thermal luminosity of a neutron star can be affected by the magnetic field. We briefly review these effects and demonstrate the influence of magnetic field strength on the thermal structure of an isolated neutron star, putting emphasis on the differences brought about by the superstrong fields and high temperatures of magnetars. For the latter objects, it is important to take proper account of a combined effect of the magnetic field on thermal conduction and neutrino emission at densities $\rho \gtrsim 10^{10}$ g cm^{-3}. We show that the neutrino emission puts a B-dependent upper limit on the effective surface temperature of a cooling neutron star.

Keywords neutron stars · dense plasmas · magnetic fields

Work supported in parts by RFBR (grants 05-02-16245 and 05-02-22003), FASI (grant NSh-9879.2006.2), and CNRS French-Russian program (grant PICS 3202)

A. Y. Potekhin
Ioffe Physico-Technical Institute, Politekhnicheskaya 26, 194021 St. Petersburg, Russia
E-mail: palex@astro.ioffe.ru

G. Chabrier
Ecole Normale Supérieure de Lyon, CRAL (UMR 5574 CNRS), 46 allée d'Italie, 69364 Lyon, France
E-mail: chabrier@ens-lyon.fr

D. G. Yakovlev
Ioffe Physico-Technical Institute, Politekhnicheskaya 26, 194021 St. Petersburg, Russia
E-mail: yak@astro.ioffe.ru

1 Introduction

Thermal emission from neutron stars can be used to measure the magnetic field, temperature, and composition of neutron-star envelopes, and to constrain the properties of matter under extreme conditions (see, e.g., Yakovlev & Pethick 2004; Yakovlev et al. 2005, and references therein). To achieve these goals, one should use reliable models of the atmosphere or condensed surface, where the thermal spectrum is formed, and of deeper layers, which provide thermal insulation of hot stellar interiors. In these layers, the effects of strong magnetic fields can be important. In recent years, significant progress has been achieved in the theoretical description of neutron-star envelopes with strong magnetic fields, but new challenges are put forward by observations of magnetars. In Sect. 2 we briefly overview recent work on the construction of models of neutron star atmospheres with strong magnetic fields and on the modeling of spectra of thermal radiation formed in an atmosphere or at a condensed surface. We list important unsolved theoretical problems which arise in this modeling. In Sect. 3, after a brief review of the effects of strong magnetic fields on the thermal structure and effective temperature of neutron stars, we describe our new calculations of the thermal structure. Compared to the previous results (Potekhin & Yakovlev 2001; Potekhin et al. 2003), we have taken into account neutrino energy losses in the outer crust of the star. We show that neutrino emission strongly affects the temperature profile in a sufficiently hot neutron star and places an upper limit on its surface temperature T_s and photon luminosity L_γ.

2 Thermal Emission from Magnetized Surface Layers of a Neutron Star

2.1 Neutron Star Atmosphere

It was realized long ago (Pavlov et al. 1995) that a neutron star atmosphere model should properly include the

effects of a strong magnetic field and partial ionization. Models of *fully ionized* neutron star atmospheres with strong magnetic fields were constructed by several research groups (e.g., Shibanov et al. 1992; Zane et al. 2000; Ho & Lai 2003, and references therein). The most recent papers highlighted the effects that can be important for atmospheres of magnetars: the ion cyclotron feature (Ho & Lai 2001; Zane et al. 2001) and vacuum polarization, including a conversion of normal radiation modes propagating in the magnetized atmosphere (Ho & Lai 2003; Lai & Ho 2003).

Early studies of *partial ionization* in the magnetized neutron star atmospheres (e.g., Rajagopal, Romani, & Miller 1997; reviewed by Zavlin & Pavlov 2002) were based on an oversimplified treatment of atomic physics and nonideal plasma effects in strong magnetic fields. At typical parameters, the effects of thermal motion of bound species are important. So far these effects have been taken into account only for hydrogen plasmas. Thermodynamic functions, absorption coefficients, the dielectric tensor and polarization vectors of normal radiation modes in a strongly magnetized, partially ionized hydrogen plasma have been obtained and used to calculate radiative opacities and thermal radiation spectra (see Potekhin et al. 2004, and references therein).

The summary of the magnetic hydrogen atmosphere models and the list of references is given by Potekhin et al. (2006). The model is sufficiently reliable at 10^{12} G $\lesssim B \lesssim 10^{13.5}$ G, i.e., in the field range typical of isolated radio pulsars. It provides realistic spectra of thermal X-ray radiation (Potekhin et al. 2004). Potekhin & Chabrier (2004) extended this model to higher B. However, there remain the following unsolved theoretical problems that prevent to obtain reliable results beyond the indicated field range.

- The calculated spectra at $B \gtrsim 10^{14}$ G depend on the adopted model of mode conversion owing to the vacuum resonance and on the description of the propagation of photons with frequencies below the plasma frequency. Neither of these problems has been definitely solved. Their solution is also important for modeling the low-frequency (UV and optical) tail of the spectrum.
- At low T or high B, hydrogen atoms recombine in H_n molecules and eventually form a condensed phase (see Sect. 2.2). Corresponding quantum-mechanical data are very incomplete.
- At 10^9 G $\lesssim B \lesssim 10^{11}$ G, transition rates of moving H atoms have not been calculated because of their complexity. There is the only one calculation of the energy spectrum of bound states appropriate to this range of B (Lozovik & Volkov 2004).
- A more rigorous treatment of radiative transfer in the atmosphere requires solving the transfer equations for the Stokes parameters which has not been done so far for partially ionized atmospheres (see, e.g., Lai & Ho 2003; van Adelsberg & Lai 2006 for the cases of fully ionized atmospheres).

Finally, we note that it is still not possible to calculate accurate atmospheric spectra at $B \gtrsim 10^{12}$ G for chemical elements other than hydrogen, because of the importance of the effects of motion of atomic nuclei in the strong magnetic fields. Apart from the H atom, these effects have been calculated only for the He atom (Al-Hujaj & Schmelcher 2003a,b), which *rests* as a whole, but has a moving nucleus, and for the He^+ ion (Bezchastnov, Pavlov, & Ventura 1998; Pavlov & Bezchastnov 2005). The data of astrophysical relevance for He^+ are partly published and partly in preparation (see Pavlov & Bezchastnov 2005); one expects to have a He/He^+ magnetic atmosphere model available in the near future.

2.2 Condensed Surface and Thin Atmosphere

The notion that an isolated magnetic neutron star has a condensed surface was first put forward by Ruderman (1971), who considered the iron surface. Lai & Salpeter (1997) and Lai (2001) studied the phase diagram of strongly magnetized hydrogen and showed that, when the surface temperature T_s falls below some critical value (dependent of B), the atmosphere can undergo a phase transition into a condensed state. A similar phase transition occurs for the equation of state of partially ionized, nonideal, strongly magnetized hydrogen plasma, constructed by Potekhin, Chabrier, & Saumon (1999) for $B \lesssim 10^{13.5}$ G and extended by Potekhin & Chabrier (2004) to the magnetar field strengths. It is analogous to the "plasma phase transition" suggested in plasma physics at $B = 0$ (see, e.g., Chabrier, Saumon, & Potekhin 2006 for discussion and references). According to Potekhin et al. (1999), the critical point for the phase transition in the hydrogen plasma is located at the density $\rho_c \approx 143 B_{12}^{1.18}$ g cm^{-3} and temperature $T_c \approx 3\times10^5 B_{12}^{0.39}$ K, where $B_{12} = B/10^{12}$ G. At $T < T_c$ the density $\rho_{\rm cond}$ of the condensed phase increases up to a few times of ρ_c. On the other hand, according to Lai (2001), the surface density of a condensed phase for heavy elements is $\rho_{\rm cond} \approx 560 A Z^{-0.6} B_{12}^{1.2}$ g cm^{-3}, where Z and A are the charge and mass numbers of the ions. These two estimates of $\rho_{\rm cond}$ are in qualitative agreement. Lai (2001) estimates the critical temperature of hydrogen as $T_c \lesssim 0.1 E_s \lesssim 10^{5.5} B_{12}^{0.4}$ K (E_s being the cohesive energy), also in agreement with the above estimate. Jones (1986) calculated the cohesive energy for Ne and Fe at 10^{12} G$\lesssim B \le 10^{13}$ G, using the density functional theory (DFT) and obtained $E_s \sim 0.1 B_{12}$ keV. Recently, Medin & Lai (2006) performed DFT calculations of the cohesive energies for zero-pressure condensed hydrogen, helium, carbon, and iron at 10^{12} G $\le B \lesssim 10^{15}$ G. For instance, they found that the cohesive energy per carbon atom ranges from ~ 50 eV at

$B = 10^{12}$ G to 20 keV at 10^{15} G. The cohesive energy per iron atom varies from ~ 0.8 keV at $B = 10^{13}$ G to 33 keV at 10^{15} G. These calculations suggest T_c of the same order of magnitude as the above estimate for hydrogen.

Note that the models of Potekhin et al. (1999) and Lai & Salpeter (1997) are constructed in the framework of the "chemical picture" of plasmas, whose validity near the plasma phase transition can be questionable (Chabrier et al. 2006). Thus the position (and the very existence) of the condensed surface requires further theoretical investigation and experimental or observational verification. Hopefully, this can be done by analyzing observations of thermal emission from neutron stars.

The thermal emission from the magnetized surface was studied by Brinkmann (1980), Turolla, Zane, & Drake (2004), Pérez-Azorín, Miralles, & Pons (2005), and van Adelsberg et al. (2005). The spectrum exhibits modest deviations from blackbody across a wide energy range, and shows mild absorption features associated with the ion cyclotron frequency (energy $\hbar\omega_{ci} = 6.3B_{12}Z/A$ eV) and the electron plasma frequency (energy $\hbar\omega_p = 28\sqrt{\rho Z/A}$ eV, where ρ is in g cm^{-3}). However, the predictions of the ion cyclotron feature and the spectrum at lower frequencies are not firm. The uncertainty arises from motion of the ions in the electromagnetic field around their equilibrium lattice positions. Most of the models treat the ions as fixed (non-moving). Only van Adelsberg et al. (2005) considered two limits of fixed and free ions. In reality, however, the ions are neither fixed nor completely free (see van Adelsberg et al. 2005 for estimates of possible uncertainties).

In addition, the condensed surface of a neutron star can be surrounded by a "thin" atmosphere, which is transparent to X-rays, but optically thick at lower wavelengths. Such a hypothesis has been first invoked by Motch, Zavlin, & Haberl (2003) for explaining the spectrum of the isolated neutron star RX J0720.4−3125. Recently, the hydrogen atmosphere model, described in Sect. 2.1, together with the condensed surface emission model of van Adelsberg et al. (2005) have been successfully used for fitting the spectrum of the isolated neutron star RX J1856.5−3754 (Ho et al. 2006) (assuming the atmosphere to be "thin" as defined above).

3 Heat Transport through Magnetized Envelopes

3.1 Overview of Previous Work

The link between the magnetized atmosphere and stellar interior is provided by a *heat blanketing (insulating) envelope*. The solution of heat transport problem relates the effective surface temperature $T_{\rm s}$ to the temperature $T_{\rm b}$ at the inner boundary of the blanketing envelope. Without a magnetic field, it is conventional to place the inner boundary at $\rho = \rho_{\rm b} = 10^{10}$ g cm^{-3}. In this case, it can be treated in the quasi-Newtonian approximation with fractional errors $\lesssim 10^{-3}$ (Gudmundsson, Pethick, & Epstein 1983). A strong magnetic field, however, greatly affects heat transport and, consequently, the thermal structure of the envelope. The thermal structure of neutron star envelopes with radial magnetic fields (normal to the surface) was studied by Van Riper (1988) (also see Van Riper 1988 for references to earlier work). His principal conclusion was that the field reduces the thermal insulation of the heat blanketing envelope due to the Landau quantization of electron motion. The thermal structure of the envelope with magnetic fields normal and tangential to the surface was analyzed by Hernquist (1985) and Schaaf (1990a). The tangential field increases the thermal insulation of the envelope, because the Larmor rotation of electrons reduces the transverse electron thermal conductivity.

The case of arbitrary angle θ_B between the field lines and the normal to the surface was studied by Greenstein & Hartke (1983) in the approximation of constant (density and temperature independent) longitudinal and transverse thermal conductivities. The authors proposed a simple formula which expresses $T_{\rm s}$ at arbitrary θ_B through two values of $T_{\rm s}$ calculated at $\theta_B = 0$ and 90°. The case of arbitrary θ_B was studied also by Schaaf (1990b) and Heyl & Hernquist (1998, 2001).

Potekhin & Yakovlev (2001) reconsidered the thermal structure of blanketing iron envelopes for any θ_B, using improved thermal conductivities (Potekhin 1999). Potekhin et al. (2003) analyzed accreted blanketing envelopes composed of light elements. In agreement with an earlier conjecture of Hernquist (1985) and simplified treatments of Page (1995) and Shibanov & Yakovlev (1996), they demonstrated that the dipole magnetic field (unlike the radial one) does not necessarily increase the total stellar luminosity L_γ at a given $T_{\rm b}$. On the contrary, the field $B \sim 10^{11}$–10^{13} G lowers L_γ, and only the fields $B \gtrsim 10^{14}$ G significantly increase it. Potekhin et al. (2003) shifted the inner boundary of the blanketing envelope to the neutron drip, $\rho_{\rm b} = 4 \times 10^{11}$ g cm^{-3}, because in some cases they found a non-negligible temperature drop at $\rho > 10^{10}$ g cm^{-3}. They obtained that magnetized accreted envelopes are generally more heat-transparent than non-accreted ones (the same is true in the field-free case, studied by Potekhin, Chabrier, & Yakovlev 1997). However, this heat transparency enhancement is less significant, when the transparency is already enhanced by a superstrong magnetic field.

Recently Potekhin, Urpin, & Chabrier (2005) showed that qualitatively the same dependence of L_γ on B and on the chemical composition holds not only for dipole, but also for small-scale field configurations.

Geppert, Küker, & Page (2004, 2006) studied heat-blanketing envelopes with a magnetic field anchored either in the core or in the inner crust of the star (with dipole and toroidal field components of different strengths). They showed that a superstrong field in the

inner crust of a not too hot star can significantly affect the surface temperature distribution and make it nonuniform and even asymmetric, with hot spots having different temperatures. Similar results were obtained by Pérez-Azorín, Miralles, & Pons (2006), who also evaluated pulsed fractions and phase-dependent spectra of neutron stars with strong magnetic fields anchored in the inner crust.

3.2 Heat-Blanketing Envelopes of Magnetars: The Effect of Neutrino Emission

Magnetars differ from ordinary pulsars in two respects: they possess superstrong surface magnetic fields, and they are generally younger and hotter. The first circumstance suggests to extend the heat-blanketing layer to deeper layers (at least to the neutron drip density as was done by Potekhin et al. 2003). The second indicates that neutrino emission can be important in the heat-blanketing envelopes. Accordingly, we have modified our computer code, which calculates the thermal structure (Potekhin & Yakovlev 2001; Potekhin et al. 2003), to make it fully relativistic and to allow for energy sinks during heat diffusion.

3.2.1 Basic Equations

A complete set of equations for mechanical and thermal structure of a spherically symmetric star in hydrostatic equilibrium has been derived by Thorne (1977). They can easily be transformed to the form valid in an envelope of a star with radial heat transport, anisotropic (slowly varying) temperature distribution over any spherical layer, and a force-free magnetic field. Assuming quasistationary heat transport and neutrino emission, these equations reduce to the following system of ordinary differential equations for the metric function (gravitational potential) Φ, the local heat flux F_r, temperature T, and gravitational mass m, contained within a sphere of circumferential radius r, as functions of pressure P:

$$\frac{\mathrm{d}\Phi}{\mathrm{d}\ln P} = -\frac{1}{\mathcal{K}_h}\frac{P}{\rho c^2}, \tag{1}$$

$$\frac{1}{r^2}\frac{\mathrm{d}(r^2F_r)}{\mathrm{d}\ln P} = \frac{P}{\rho g}\frac{Q}{\mathcal{K}_h\mathcal{K}_g} - 2F_r\frac{\mathrm{d}\Phi}{\mathrm{d}\ln P}, \tag{2}$$

$$\frac{\mathrm{d}\ln T}{\mathrm{d}\ln P} = \frac{3}{16}\frac{F_r}{\sigma T^4}\frac{K'P}{g}\frac{1}{\mathcal{K}_h\mathcal{K}_g} - \frac{\mathrm{d}\Phi}{\mathrm{d}\ln P}, \tag{3}$$

$$\frac{\mathrm{d}r}{\mathrm{d}\ln P} = -\frac{P}{\rho g}\frac{\mathcal{K}_r}{\mathcal{K}_h\mathcal{K}_g}, \tag{4}$$

$$\frac{\mathrm{d}m}{\mathrm{d}\ln P} = -\frac{4\pi r^2 P\mathcal{K}_r}{g\mathcal{K}_h\mathcal{K}_g}. \tag{5}$$

Here ρ is the mass density (equivalent energy density of the matter), Q is the net energy loss per unit volume ($Q = Q_\nu$ is the neutrino emissivity in our case, although generally $Q = Q_\nu - Q_\mathrm{h}$, Q_h being the heat deposition rate, e.g., due to nuclear reactions), $K' = K\rho_\mathrm{bar}/\rho$, K is the opacity, $\rho_\mathrm{bar} = n_\mathrm{bar}m_\mathrm{H}$ is the so-called "baryon mass density," n_bar is the baryon number density, m_H is the mass of the hydrogen atom, σ is the Stefan-Boltzmann constant, $g = Gm/(r^2\mathcal{K}_r)$ is the local gravity, and G is the gravitational constant. Furthermore,

$$\mathcal{K}_r = (1 - 2Gm/rc^2)^{1/2}, \tag{6}$$

$$\mathcal{K}_h = 1 + P/\rho c^2, \tag{7}$$

$$\mathcal{K}_g = 1 + 4\pi r^3 P/mc^2, \tag{8}$$

are general relativistic corrections to radius, enthalpy and surface gravity, respectively. We adopt the conventional definition of the opacity K, used also by Thorne (1977). In our notations $K' = 16\sigma T^3/(3\kappa\rho)$, where κ is the total (electron plus radiative) thermal conductivity of the plasma. Note that $\rho \approx \rho_\mathrm{bar}$ and $K' \approx K$ in the entire neutron star envelope. We use the same thermal conductivities as in Potekhin & Yakovlev (2001). The effective radial thermal conductivity in a local part of the surface equals $\kappa = \kappa_\parallel \cos^2\theta_B + \kappa_\perp \sin^2\theta_B$, where $\kappa_\parallel$ and $\kappa_\perp$ are the components of the conductivity tensor responsible for heat transport along and across field lines, respectively.

The local (non-neutrino) luminosity equals the integral of the flux over the sphere of radius r,

$$L_r = \int \sin\theta \mathrm{d}\theta\, \mathrm{d}\varphi\, r^2 F_r(\theta,\varphi), \tag{9}$$

where (θ,φ) are the polar and azimuthal angles. For a magnetic dipole model (Ginzburg & Ozernoy 1964), $\tan\theta = 2\tan\theta_B$.

The boundary conditions to Eqs. (1)–(5) are

$$\Phi_\mathrm{s} = \ln\mathcal{K}_{rs},\ F_{r\mathrm{s}} = F_R = \sigma T_\mathrm{s}^4,\ r_\mathrm{s} = R,\ m_\mathrm{s} = M,$$

and the surface pressure is determined, following Gudmundsson, Pethick, & Epstein (1983), by the condition $K_{\mathrm{rad,s}}P_\mathrm{s}/g_\mathrm{s} = 2/3$, where K_rad is the radiative opacity. The subscript 's' refers to surface values; M is the gravitational stellar mass.

General Relativity correction factors $\mathcal{K}_r$, $\mathcal{K}_h$, and $\mathcal{K}_g$ in Eqs. (6)–(8) are nearly constant because $(M - m)/M \sim 10^{-5}$ and $P/\rho c^2 \sim 10^{-2}$ at the bottom of the outer crust. However, they are taken into account in our code, in order to extend calculations to deeper neutron star layers, when required.

Equations (2), (3) are one-dimensional, which implies that the mean temperature gradient along stellar radius is large compared to the tangential temperature gradient, i.e., $\epsilon \equiv |\partial T/\partial x|/|\partial T/\partial r| \ll 1$, where x is a coordinate along the stellar surface. Let us roughly estimate the mean value of ϵ for a large-scale (e.g., dipole) magnetic field, following Greenstein & Hartke (1983). In this case, $\epsilon \sim (\bar{T}_\mathrm{s}/T_0)(l_0/R)$, where l_0 is the depth at which the temperature distribution becomes nearly isotropic ($T = T_0$ at the depth l_0) and $\bar{T}_\mathrm{s}$ is the mean surface

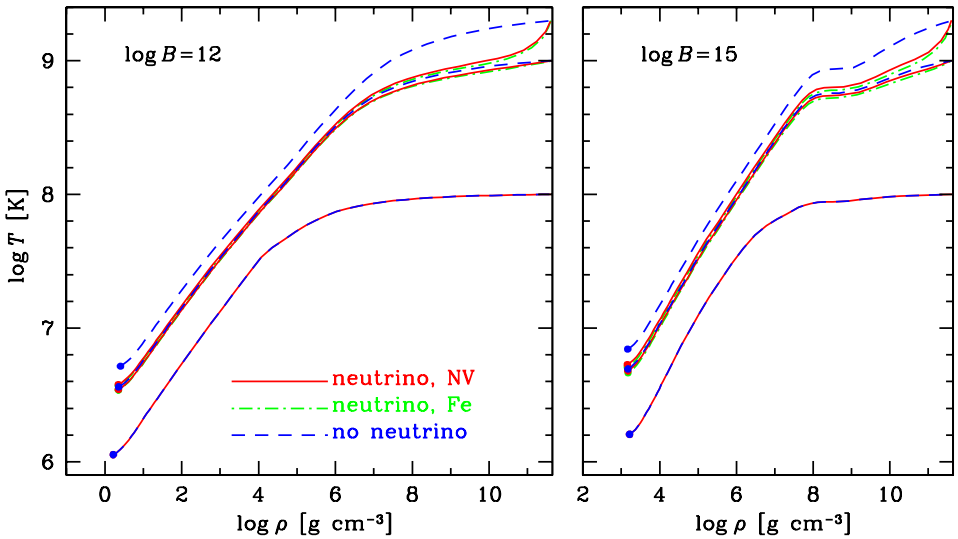

Fig. 1 Temperature profiles in the outer crust of a neutron star with magnetic field $B = 10^{12}$ G (left panel) or $B = 10^{15}$ G (right panel), directed perpendicular to the stellar surface ($\theta_B = 0$). Solid lines (NV) – ground-state (Negele–Vautherin) nuclear composition of the envelope, dot-dashed lines – ^{56}Fe envelope. For comparison, dashed lines show the temperature profiles without allowance for neutrino emission (for ground-state matter). For every family of curves, temperature at the neutron drip density is fixed to $T_\mathrm{b} = 10^8$ K, 10^9 K, and 2×10^9 K. The dots at the left end of the profiles correspond to the radiative surface, where the optical depth equals 2/3 and $\sigma T^4 = F_R$.

temperature. At the bottom of the outer crust (i.e., assuming $T_0 = T_\mathrm{b}$) we have $l_0/R \lesssim 0.1$ (e.g., $l_0 \approx 0.6$ km for $M = 1.4 M_\odot$ and $R = 10$ km) and $T_\mathrm{s}/T_0 \sim 10^{-2}$ (see Sect. 3.2.2). This estimate gives $\epsilon \lesssim 10^{-3}$.

Nevertheless, the one-dimensional approximation is inaccurate at those loci where magnetic field lines are tangential to the surface, because in this case one cannot neglect their curvature, $\partial\theta_B/\partial x$. For large-scale magnetic field ($\partial\theta_B/\partial x \sim R^{-1}$), the maximum size a of such sites can be estimated as the distance at which an initially tangential field line crosses the depth l_0 (which assumes that heat flows along field lines, i.e., $\kappa_\perp/\kappa_\parallel \ll l_0/a$). Thus, $a \lesssim \sqrt{R l_0}$. Since T_s is minimal at such sites, their contribution to the total stellar luminosity can be neglected in the first approximation.

3.2.2 Results

We have solved Eqs. (1) – (5) using a straightforward generalization of the Runge-Kutta method employed in our previous papers (Potekhin et al. 1997; Potekhin & Yakovlev 2001; Potekhin et al. 2003). Temperature profiles have been calculated within a local part of the blanketing envelope with a locally constant magnetic field. At every value of P, a corresponding value of ρ was found from the equation of state of magnetized electron-ion relativistic plasma (e.g., Potekhin & Yakovlev 1996), using approximations of Fermi-Dirac integrals presented in Potekhin & Chabrier (2000). In all examples shown in the figures we chose the "canonical" neutron star mass $M = 1.4 M_\odot$ and radius $R = 10$ km. The neutrino emissivity is calculated as $Q_\nu = Q_\mathrm{pair} + Q_\mathrm{pl} + Q_\mathrm{syn} + Q_\mathrm{brems}$, where the contributions due to electron-positron pair annihilation Q_pair, plasmon decay Q_pl, synchrotron radiation of neutrino pairs by electrons Q_syn, and bremsstrahlung in electron-nucleus collisions Q_brems are given, respectively, by Eqs. (22), (38), (56), and (76) of Yakovlev et al. (2001). According to the results of Itoh et al. (1996) and Yakovlev et al. (2001), other neutrino emission mechanisms are unimportant in the outer crust of neutron stars.

Our calculations show that neutrino emission is crucially important for the thermal structure of neutron stars with internal temperature $T_\mathrm{b} \gtrsim 10^9$ K.

Figure 1 shows temperature profiles at $T_\mathrm{b} = 10^8$ K, 10^9 K, and 2×10^9 K for magnetic fields $B = 10^{12}$ G and 10^{15} G, directed perpendicular to the stellar surface. The present results (solid and dot-dashed lines) are compared with the profiles calculated neglecting neutrino emission (dashed lines). At the lowest temperature $T_\mathrm{b} = 10^8$ K there is virtually no difference (all the lines coincide). At $T_\mathrm{b} = 10^9$ K, the difference is noticeable, and at $T_\mathrm{b} = 2 \times 10^9$ K it is large. Because of the growth of neutrino emission with increasing temperature at $\rho \gtrsim 10^{10}$ g cm^{-3}, T_s is nearly independent of T_b at $T_\mathrm{b} \gtrsim 10^9$ K, but depends on the magnetic field.

In this figure we also compare temperature profiles for the different heavy-element compositions of the outer envelope: iron (dot-dashed lines) and ground-state matter (Negele & Vautherin 1973). The effect of composition is not strong, but noticeable when the neutrino emission is important, because Q_ν depends on the electron number density that is a function of composition for a given ρ.

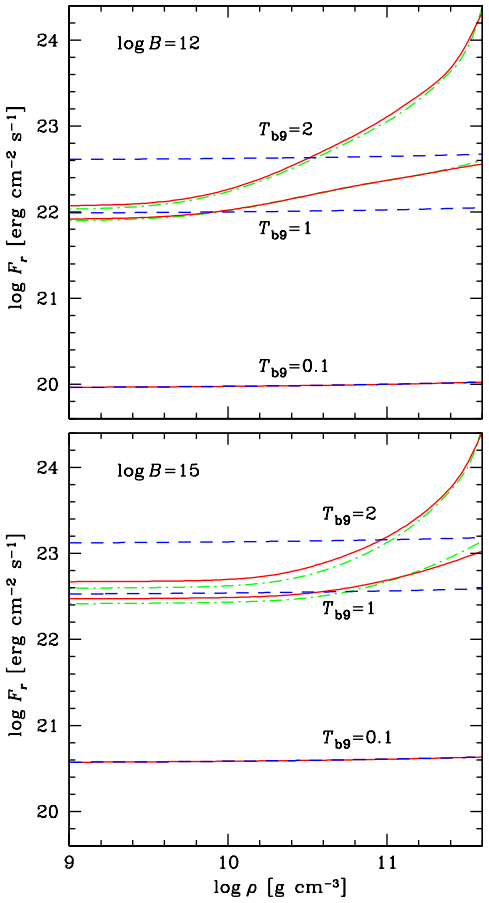

Fig. 2 Profiles of local radial heat flux F_r for the cases shown in Fig. 1. Top panel: $B = 10^{12}$ G, bottom panel: $B = 10^{15}$ G; solid lines – ground-state matter, dot-dashed lines – ^{56}Fe, dashed lines – without neutrino emission for ground-state matter.

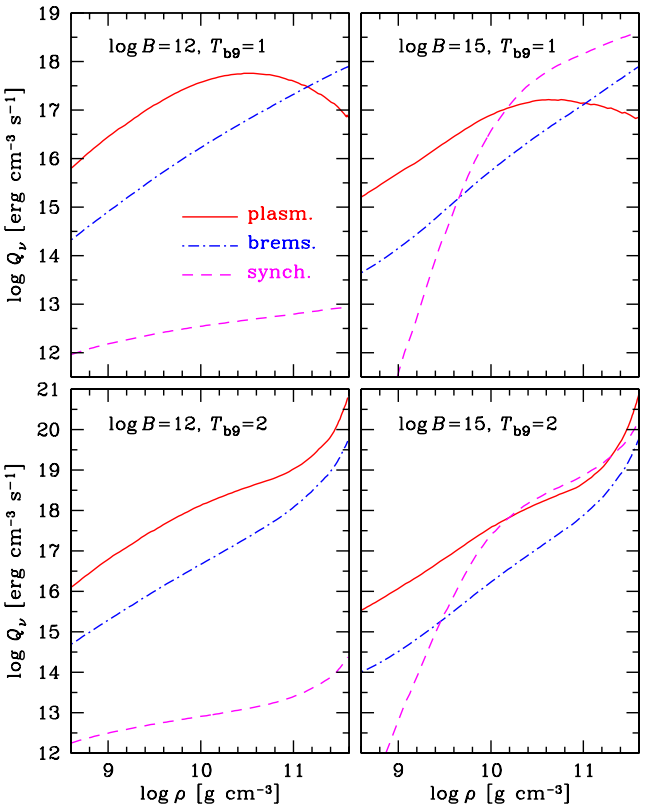

Fig. 3 Contributions to the total neutrino emissivity Q_ν from plasmon decay (solid lines), electron neutrino bremsstrahlung (dot-dashed lines), and electron synchrotron radiation (dashed lines). Left panels: $B = 10^{12}$ G (radial field); right panels: $B = 10^{15}$ G; top panels: $T = 10^9$ K; bottom panels: $T = 2 \times 10^9$ K.

Figure 2 demonstrates the profile of the local heat flux F_r, for the same cases as in Fig. 1, plotted by the same line types. Without neutrino emission (dashed lines), F_r would be nearly constant, with only $\approx 2\%$ increase towards the inner crust due to the General Relativity effects (associated with the variation of the metric function Φ) and $\approx 9\%$ increase because of the spherical geometry (the r^2 factor). The neutrino emission leads to a strong dependence of the flux on ρ and violates the familiar relation between F_r and T_s derived in the absence of energy sinks.

Figure 3 shows which neutrino emission mechanism dominates at given ρ, T_b, and B. For superstrong magnetic fields, the neutrino synchrotron mechanism dominates in certain density ranges, which does not happen at "ordinary pulsar" $B \sim 10^{12}$ G. It is natural because of the strong B-dependence of the synchrotron neutrino emissivity. Pair annihilation neutrino emissivity is not seen in the figure, because it is too small. Notice that the emissivity of plasmon decay and bremsstrahlung processes can be affected by superstrong magnetic fields which has not been explored so far (and we present the emissivities in the field-free case). A slow dependence of these emissivities on B, seen in Fig. 3, is indirect (caused by the dependence of temperature profiles on B).

Figures 4 and 5 give the $T_\mathrm{s}(T_\mathrm{b})$ relation for the magnetic fields $B = 10^{12}$ G and $B = 10^{15}$ G perpendicular and parallel to the radial direction. The relations obtained with and without allowance for neutrino emission are plotted by solid and dashed lines, respectively. We see that at $T_\mathrm{b} \lesssim 10^8$ K the neutrino emission does not affect T_s. At higher $T_\mathrm{b} \gtrsim 10^9$ K, in contrast, this emission is crucial: if $Q_\nu = 0$, then T_s continues to grow up with increasing T_b, whereas with realistic Q_ν the surface temperature tends to a constant limit, which depends on θ_B and B. In most cases this limit is reached when $T_\mathrm{b} \sim 10^9$ K, but for a superstrong field (right panel) and transverse heat propagation, it is reached at still smaller $T_\mathrm{b} \sim 3 \times 10^8$ K.

In Fig. 6 we explore joint effects of magnetic field, neutrino emission, and the shift of the inner boundary from 10^{10} g cm^{-3} to the neutron drip. Here magnetic field lines are directed along the surface (perpendicular to the direction of heat transport). Therefore, these

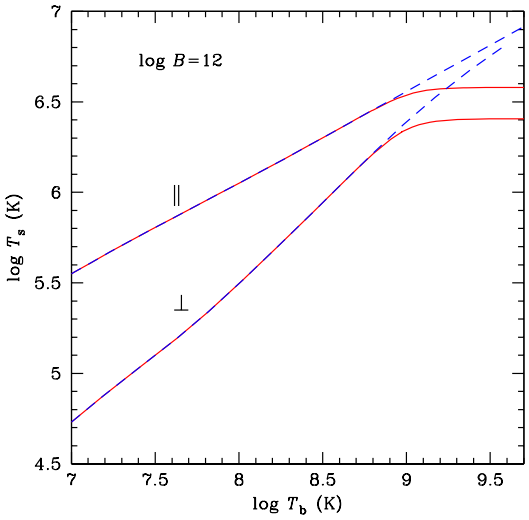

Fig. 4 Surface temperature $T_{\rm s}$ as a function of temperature $T_{\rm b}$ at the neutron drip point for a neutron star with the magnetic field $B = 10^{12}$ G, directed along stellar radius ($\theta_B = 0$, parallel heat transport, sign $\|$) or along the surface ($\theta_B = 90^\circ$, transverse transport, $\perp$). Ground-state composition is assumed. Solid lines – present calculation, dashed lines – neutrino emission is neglected.

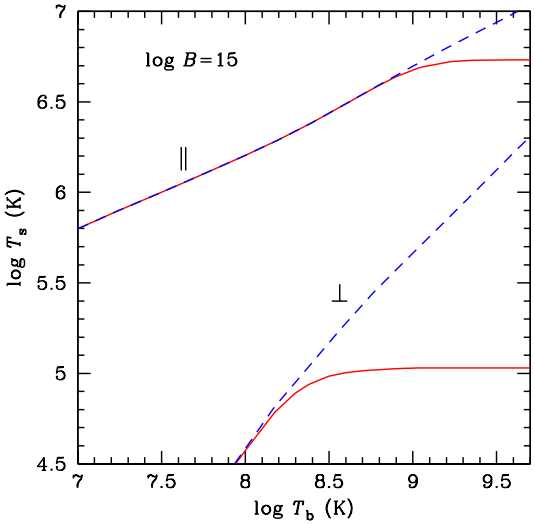

Fig. 5 The same as in Fig. 4, but for $B = 10^{15}$ G.

effects are most pronounced. The solid lines are the results of accurate calculations; the dashed lines, as before, show the model with $Q_\nu = 0$; and dot-dashed lines are obtained by solving Eqs. (1) – (5) in the whole domain $\rho_{\rm s} \le \rho \le 4 \times 10^{11}$ g cm^{-3}, but with the magnetic field artificially "switched off" at $\rho > 10^{10}$ g cm^{-3}. This is a simulation of the model, where the heat transport in the magnetized plasma is solved accurately up to $\rho_{\rm b} = 10^{10}$ g cm^{-3}, while after this boundary nonmagnetic heat balance and transport equations are solved. In the absence of the results reported here, the latter model was used by Kaminker et al. (2006) to study the thermal structure and evolution of magnetars as cooling neutron stars with a phenomenological heat source in a spherical internal layer. In the left panel of Fig. 6, the solid and dot-dashed lines almost coincide, indicating that in this case $\rho_{\rm b} = 10^{10}$ g cm^{-3} may provide a sufficient accuracy. In the right panel, in contrast, the effect of the shift of the inner boundary is quite visible. Therefore, we conclude that the development of our thermal structure code, reported here, will allow us to study the thermal history of magnetars at a higher accuracy level.

Meanwhile, a comparison of the profiles shown in Figs. 1 and 6 prompts that at $T \gtrsim 10^9$ K and $B \sim 10^{15}$ G the magnetic effects on the conductivity could be important at still higher densities in the inner crust. Investigation of this possibility requires taking into account the effects of free (possibly superfluid) neutrons on thermal conduction and neutrino emission. We are planning to perform such study in the future.

In the above figures we have shown the results of calculations where the surface of a neutron star was assumed diffuse, i.e., without the phase transition discussed in Sect. 2.2. However, for $B = 10^{15}$ G and $T_{\rm b} \lesssim 10^9$ K the surface temperature $T_{\rm s}$ is below the estimates of the critical temperature T_c given in Sect. 2.2. This possibility is explored in Fig. 7. Here we use the equation of state containing nonideal terms for strongly magnetized fully ionized plasma (Sect. IIIB of Potekhin et al. 1999), which enforce the phase transition. At $B = 10^{15}$ G the surface density is very high, $\rho_{\rm cond} \approx 3.1 \times 10^7$ g cm^{-3}, in our model (and the analytic estimate in Sect. 2.2 gives $\rho_{\rm cond} \sim 2 \times 10^7$ g cm^{-3}). The solid lines in the left panels reproduce the profiles shown in Figs. 1 and 6, whereas the dot-dashed lines display the case of magnetic condensation. In the right panels, we show the same temperature profiles as a function of local proper depth l ($\mathrm{d}l = -\mathcal{K}_r^{-1}\mathrm{d}r$), measured from the radiative surface. Although the temperature profiles with and without magnetic condensation are drastically different in the surface layers, the effective temperature remains almost the same. Thus, the magnetic condensation does not significantly affect the $T_{\rm s}(T_{\rm b})$ relation. This should not be surprising, because, as explained by Gudmundsson et al. (1983), the main regulator of the $T_{\rm b} - T_{\rm s}$ relation is the "sensitivity strip" where κ has a minimum. This domain, a real bottleneck for the heat outflow, lies at $\rho > \rho_{\rm cond}$ (except for low $T_{\rm s}$, not considered here), and therefore it is not affected by the condensation.

4 Summary

We have described the main effects of strong magnetic fields on the properties of neutron star atmospheres and heat blanketing envelopes, with the emphasis on the difference between ordinary neutron stars and magnetars. Observations of magnetars pose new theoretical problems and challenges because of magnetars' superstrong

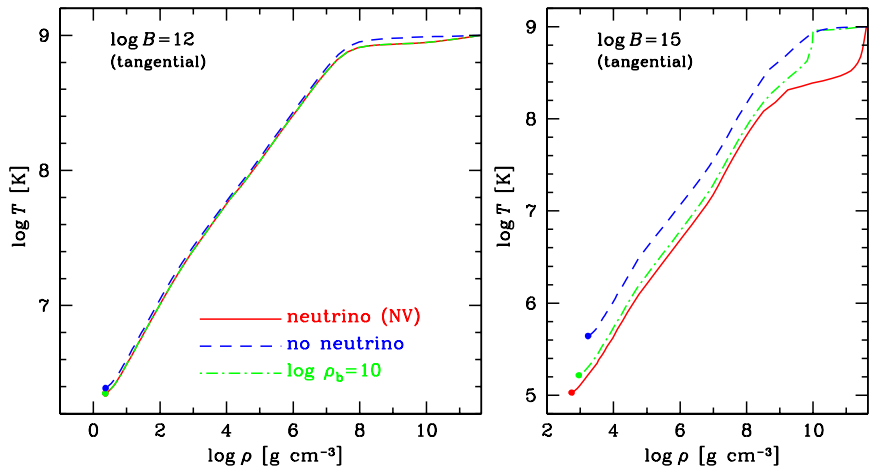

Fig. 6 Temperature profiles in the outer crust of a neutron star with the magnetic field $B = 10^{12}$ G (left panel) or $B = 10^{15}$ G (right panel), directed parallel to the stellar surface, with the temperature $T_{\rm b} = 10^9$ K at neutron drip density and the ground-state composition of the matter. Solid lines – present calculation, dot-dashed lines – with a switch to non-magnetic ($B = 0$) calculation at $\rho > 10^{10}$ g cm^{-3}, dashed lines – without neutrino energy losses.

magnetic fields and high temperatures. We also report a solution to one of such problems, which consists in taking into account neutrino energy losses in the outer crust of hot, strongly magnetized neutron stars. We have demonstrated that, because of these losses, the effective surface temperature $T_{\rm s}$ almost ceases to depend on the temperature $T_{\rm b}$ in the inner crust as soon as $T_{\rm b}$ exceeds 10^9 K. A direct consequence of this observation is that in the absence of powerful energy sources in outer envelopes, the stationary (time-averaged) effective temperature cannot be raised above the value that it would have at $T_{\rm b} \approx 10^9$ K, irrespectively of the energy release in the deeper layers.

Acknowledgements We are grateful to the anonymous referee for useful comments. We thank A.D. Kaminker for pointing out to some misprints in formulae, which are corrected in this electronic version of the paper. AYP thanks the organizers of the conference "Isolated Neutron Stars: from the Interior to the Surface" (London, April 24–28, 2006), especially Silvia Zane and Roberto Turolla, for perfect organization, attention and support. Fruitful discussions with participants of this conference have significantly contributed to the developments partly reported in the present paper.

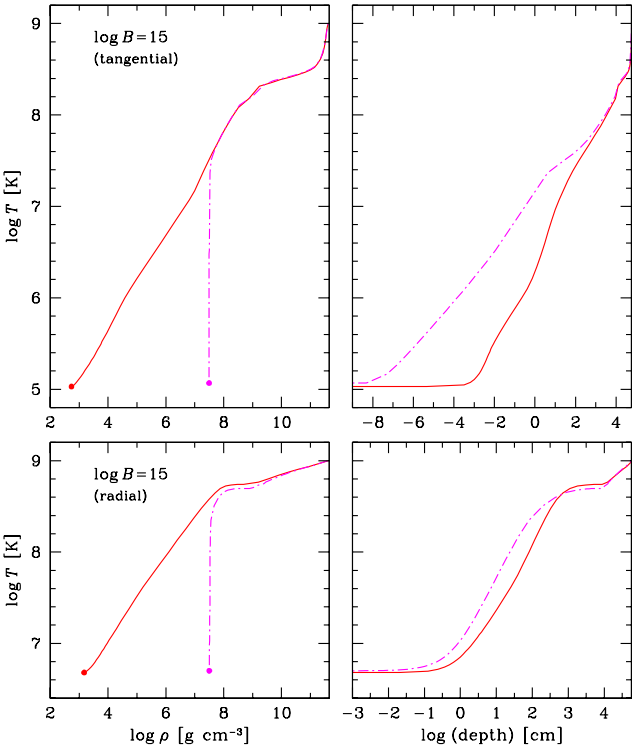

Fig. 7 Temperature in the outer crust of a neutron star as a function of density (left panels) or proper depth behind the radiative surface (right panels). Magnetic field $B = 10^{15}$ G is directed parallel (top panels) or perpendicular (bottom panels) to the stellar surface; $T_{\rm b} = 10^9$ K. Solid lines – the model of diffuse surface (no phase transition), dot-dashed lines – condensed surface.

References

Al-Hujaj O.-A. & Schmelcher P.: Phys. Rev. A **67**, 023403 (2003a)
Al-Hujaj O.-A. & Schmelcher P.: Phys. Rev. A **68**, 053403 (2003b)
Bezchastnov V.G., Pavlov G.G., & Ventura J.: Phys. Rev. A **58**, 180 (1998)
Brinkmann W.: A&A **82**, 352 (1980)
Chabrier G., Saumon D., & Potekhin A.Y.: J. Phys. A: Math. Gen., **39**, 4411
Geppert U., Küker M., & Page D.: A&A, **426**, 267 (2004)

Geppert U., Küker M., & Page D.: A&A, **457**, 957 (2006)
Ginzburg V.L., Ozernoy L.M., 1964, Zh. Eksp. Teor. Fiz., 47, 1030 (English translation: Sov. Phys. – JETP, 20, 689)
Greenstein G. & Hartke G.J.: ApJ, **271**, 283 (1983)
Gudmundsson E.H., Pethick C.J., & Epstein R.I.: ApJ, **272**, 286 (1983)
Hernquist L.: MNRAS, **213**, 313 (1985)
Heyl J.S. & Hernquist L.: MNRAS, **300**, 599 (1998)
Heyl J.S. & Hernquist L.: MNRAS, **324**, 292 (2001)
Ho W.C.G. & Lai D.: MNRAS, **327**, 1081 (2001)
Ho W.C.G. & Lai D.: MNRAS, **338**, 233 (2003)
Ho W.C.G., Kaplan D.L., Chang P., van Adelsberg M., & Potekhin A.Y.: Thin magnetic hydrogen atmospheres and the neutron star RX J1856.5−3754. This volume (2006)
Itoh N., Hayashi H., Nishikawa A., & Kohyama Y.: ApJS **102**, 411 (1996)
Jones P.B.: MNRAS, **218**, 477 (1986)
Kaminker A.D., Yakovlev D.G., Potekhin A.Y., Shibazaki N., Shternin P.S., & Gnedin O.Y.: Cooling of magnetars with internal layer heating. This volume (2006)
Lai D.: Rev. Mod. Phys. **73**, 629 (2001)
Lai D. & Ho W.C.G.: ApJ **588**, 962 (2003)
Lai D. & Salpeter E.E.: ApJ **491**, 270 (1997)
Lozovik Yu.E. & Volkov S.Yu.: Phys. Rev. A, **70**, 023410 (2004)
Medin Z. & Lai D.: Density-functional-theory calculations of matter in strong magnetic fields: II. Infinite chains and condensed matter. Phys Rev A, submitted. Preprint astro-ph/0607277 (2006)
Motch C., Zavlin V.E., & Haberl F.: A&A, **408**, 323 (2003)
Negele J.W. & Vautherin D.: Nucl. Phys., **A207**, 298 (1973)
Page D.: ApJ, **442**, 273 (1995)
Pavlov G.G. & Bezchastnov V.G.: ApJ, **635**, L61 (2005)
Pavlov G.G., Shibanov Yu.A., Zavlin V.E., & Meyer R.D.: Neutron star atmospheres. In: Alpar M.A., Kiziloğlu Ü., van Paradijs, J. (eds.) The Lives of the Neutron Stars, Proceedings of the NATO ASI Ser. C, **450**, p. 71. Kluwer, Dordrecht (1995)
Pérez-Azorín J.F., Miralles J.A., & Pons J.A.: A&A **433**, 275 (2005)
Pérez-Azorín J.F., Miralles J.A., & Pons J.A.: A&A **451**, 1009 (2006)
Potekhin A.Y.: A&A, **351**, 787 (1999)
Potekhin A.Y. & Chabrier G.: Phys. Rev. E **62**, 8554 (2000)
Potekhin A.Y. & Chabrier G.: ApJ **600**, 317 (2004)
Potekhin A.Y. & Yakovlev D.G.: A&A, **314**, 341 (1996)
Potekhin A.Y. & Yakovlev D.G.: A&A, **374**, 213 (2001)
Potekhin A.Y., Chabrier G., & Yakovlev D.G.: A&A, **323**, 415 (1997)
Potekhin A.Y., Chabrier G., & Shibanov Yu.A.: Phys. Rev. E, **60**, 2193 (1999)
Potekhin A.Y., Yakovlev D.G., Chabrier G., & Gnedin O.Y.: ApJ, **594**, 404 (2003)
Potekhin A.Y., Lai D., Chabrier G., & Ho W.C.G.: ApJ **612**, 1034 (2004)
Potekhin A.Y., Urpin V.A., & Chabrier G.: A&A, **443**, 1025 (2005)
Potekhin A.Y., Chabrier G., Lai D., Ho W.C.G., & van Adelsberg M.: J. Phys. A: Math. Gen., **39**, 4453 (2006)
Rajagopal M., Romani R., & Miller M.C.: ApJ, **479**, 347 (1997)
Ruderman M.: Phys. Rev. Lett., **27**, 1306 (1971)
Schaaf M.E.: A&A, **227**, 61 (1990a)
Schaaf M.E.: A&A, **235**, 499 (1990b)
Shibanov Yu.A., & Yakovlev D.G.: A&A, **309**, 171 (1996)
Shibanov Yu.A., Zavlin V.E., Pavlov G.G., Ventura J.: A&A, **266**, 313 (1992)
Thorne K.S.: ApJ **212**, 825 (1977)
Turolla R., Zane S., & Drake J.J.: ApJ, **603**, 265 (2004)
van Adelsberg M. & Lai D.: Atmosphere models of magnetized neutron stars: QED effects, radiation spectra, and polarization signals. MNRAS, accepted. Preprint astro-ph/0607168 (2006)
van Adelsberg M., Lai D., Potekhin A.Y., & Arras P.: ApJ, **628**, 902 (2005)
Van Riper K.A.: ApJ, **329**, 339 (1988)
Yakovlev D.G. & Pethick C.: ARA&A, **42**, 169 (2004)
Yakovlev D.G., Kaminker A.D., Gnedin O.Y., & Haensel P.,: Phys. Rep., **354**, 1 (2001)
Yakovlev D.G., Gnedin O.Y., Gusakov M.E., Kaminker A.D., Levenfish K.P., & Potekhin A.Y.: Nucl. Phys. A, **752**, 590 (2005)
Zane S., Turolla R., & Treves A.: ApJ, **537**, 387 (2000)
Zane S., Turolla R., Stella L., & Treves A.: ApJ, **560**, 384 (2001)
Zavlin V.E. & Pavlov G.G.: Modeling neutron star atmospheres. In: Becker W., Lesch H., Trümper J. (eds.) Proceedings of the 270. WE-Heraeus Seminar on Neutron Stars, Pulsars, and Supernova Remnants, MPE Report 278, p. 263. MPE, Garching (2002)